Chemical Engineering Journal 466 (2023) 143048

Contents lists available at ScienceDirect

Chemical Engineering Journal

journal homepage: www.elsevier.com/locate/cej

Highly propylene-selective asymmetric mixed-matrix membranes by polymer phase-inversion in sync with *in-situ* ZIF-8 formation

Yinying Hua [a,1], Sunghwan Park [a,b,1], Gyeong Min Choi [c], Ho Jin Jung [c], Kie Yong Cho [c], Hae-Kwon Jeong [a,d,*]

[a] *Artie McFerrin Department of Chemical Engineering, Texas A&M University, 3122 TAMU, College Station, TX 77843-3122, United States*
[b] *School of Energy Materials & Chemical Engineering, Kyungpook National University, 2559 Gyeongsang-daero, Sangju-si, Gyeongsangbuk-do 37224, Republic of Korea*
[c] *Department of Industrial Chemistry, Pukyong National University, 45 Yongso-ro, Nam-gu, Busan 48513, Republic of Korea*
[d] *Department of Materials Science and Engineering, Texas A&M University, 3122 TAMU, College Station, TX 77843-3122, United States*

ARTICLE INFO

Keywords:
Mixed-matrix membranes
Metal–organic frameworks
Zeolitic-imidazolate frameworks
Gas separations
Propylene/propane separation

ABSTRACT

Although mixed-matrix membranes (MMMs) have been extensively studied, their commercial applications have been hampered by scientific and engineering challenges. Herein, we report an innovative one-step MMM fabrication method that can put the commercialization of MMMs forward by overcoming most of the current challenges because it enables the rapid formation of high-performance asymmetric MMMs in a scalable manner. The method termed phase-inversion in sync with metal–organic framework (MOF) formation (PIMOF) involves a polymer film undergoing phase inversion and simultaneously ZIF-8 nanoparticles forming *in-situ* inside the polymer. The resulting MMMs show unexpectedly high C_3H_6/C_3H_8 separation performances (C_3H_6 permeance of ca. 7.5 GPU and C_3H_6/C_3H_8 separation factor of ca. 107), which is attributed mostly to the high effective ZIF-8 loading (>50 wt%) and the enhanced molecular sieving effect of the unusually small sub-5 nm ZIF-8 filler nanoparticles by restricted linker motion.

1. Introduction

Membrane-based gas separation is an attractive energy-efficient alternative to the conventional thermally-driven technologies [1,2]. Several polymer membranes have successfully been applied for the commercial separations of light gases [3]. The separation performances of the polymer membranes are, however, limited by a trade-off between permeability and selectivity [4], thereby hindering their applications for rapidly growing diverse gas separation markets such as olefin/paraffin separations [3,5]. As such, a great deal of efforts have been made to improve the separation performances of polymer membranes by adding more selective and/or permeable filler particles, so called mixed-matrix membranes (MMMs) [6]. While current MMMs have shown improved gas separation performances compared to their polymer counterparts, the commercial applications of the MMMs have been substantially hampered by several engineering and scientific challenges [7–9]. Some of the scientific challenges include compatibility and interfacial structures between polymer and filler phases and their uniform mixing [10]. The engineering challenges have to do with the fabrication of MMMs in a scalable geometry (i.e., asymmetric microstructures with thin selective mixed-matrix layers), which turns out extremely complex and requires precise control of various parameters to incorporate fillers into a sub-micron thick skin layer [11]. There have been tremendous efforts to address the scientific challenges including poor filler-polymer interfacial interactions and filler agglomeration [12]. On the other hand, much less attention has been given to the engineering challenges for economically manufacturing defect-free MMMs [7]. The engineering challenges result mostly from the conventional physical blending based MMM processing, by which it turns out extremely difficult to rapidly prepare asymmetric membranes with thin selective mixed-matrix layers. It is, therefore, highly desirable to develop a fundamentally new MMM fabrication strategy that can overcome both of the scientific and engineering challenges.

In-situ MMM fabrication is an emerging strategy that might potentially overcome the limitations of the conventional blending methods. In this regard, metal–organic frameworks (MOFs) offer unique opportunity

* Corresponding author at: Artie McFerrin Department of Chemical Engineering, Texas A&M University, 3122 TAMU, College Station, TX 77843-3122, United States.
E-mail address: hjeong7@tamu.edu (H.-K. Jeong).
[1] These authors contributed equally to this work.

https://doi.org/10.1016/j.cej.2023.143048
Received 1 January 2023; Received in revised form 19 March 2023; Accepted 15 April 2023
Available online 17 April 2023

for *in-situ* MMM fabrication due to their labile chemistry and organic moieties that are compatible with polymers. Marti et al. [13] demonstrated a simple one-step fabrication of Matrimid®/UiO-66 MMMs using *in-situ* filler formation in a polymer solution containing UiO-66 precursors. Despite facile MMM formation, the membranes showed limited filler loadings due to the particle agglomeration, exhibiting not much improvement in their gas separation performances as compared to those conventionally prepared [13]. Inspired by the rhizobium-inducing nodule for integrated symbiosis, He et al. [14] developed a strategy to fabricate MMMs with ultrahigh ZIF-8 loading up to 67.2 wt%. By adding ZIF-8 precursors into PIM-1/$CHCl_3$ solution, nano-sized particles were formed in the aqueous phase of an oil–water mixture. The ZIF-8/PIM-1 floccules were collected and redissolved to be casted into membrane. The synthesized symmetric MMM showed outstanding CO_2 permeability of 6,338 Barrer. Recently, our group reported a novel scalable *in-situ* MMM fabrication strategy, termed as polymer-modification-enabled metal–organic framework formation (PMMOF) [15]. The PMMOF decouples filler incorporation from membrane formation by *in-situ* forming MOF fillers in preformed polymer films, thereby enabling the transformation of polymer membranes to MMMs [15]. Although the PMMOF process effectively addressed several issues of conventional blending-based processing, the process involves multiple steps (i.e., hydrolysis, ion-exchange, ligand treatment, and imidization), likely adding the manufacturing cost. More importantly, the PMMOF can be applied only to polyimide-based polymers, compromising its versatility.

Here, we present a novel approach for scalable *in-situ* MMM fabrications, termed as phase-inversion in sync with MOF formation (PIMOF), completely different from our previous PMMOF, which successfully addresses the above-mentioned issues inhibiting the commercial applications of MMMs. The PIMOF enabled one-step facile preparation of ZIF-8-containing MMMs, exhibiting an asymmetric structure with defect-free ultra-thin selective mixed-matrix skin layers on top of porous supportive layers. The resulting MMMs by PIMOF showed exceptional propylene/propane separation performances compared with any propylene-selective MMMs reported so far. The unexpectedly high separation performances of the MMMs were attributed to the high loading of surprisingly small ZIF-8 fillers *in situ* formed inside polymer and the reduced effective aperture resulting from the restricted linker swing motion.

2. Experimental

2.1. Materials and methods

4,4-(Hexafluoroisopropylidene) diphthalic anhydride 2,4,6-trimethyl-1,3-phenylenediamine (6FDA-DAM) (Mw: 148 k, PDI: 2.14) was purchased from Akron Polymer Systems Inc. 1-methyl-2-pyrrolidone (NMP, C_5H_9NO, >99.0 %, Sigma-Aldrich), tetrahydrofuran (THF, C_4H_8O, >99.0 %, Alfa Aesar), methanol (MeOH, CH_3OH, >99.8 %, VWR International), ethanol (EtOH, C_2H_5OH, 94–96 %, Alfa Aesar), zinc nitrate hexahydrate (ZnN, $Zn(NO_3)_2{\cdot}6H_2O$, 98 %, Sigma-Aldrich), and 2-methylimidazole (HmIm, $C_4H_6N_2$, 99 %, Sigma-Aldrich) were used. All chemicals were used as received without further purification.

2.2. Fabrication of polymer and mixed-matrix membranes

A polymer solution was prepared by dissolving 15 wt% of 6FDA-DAM in 40.7 w% NMP and 20.3 wt% THF, followed by addition of non-solvent additives of 6 wt% ZnN and 18 wt% EtOH. The solution was shaken on a lab shaker overnight at room temperature until it became homogeneous. The homogenous polymer solution was then casted with thickness of ~470 μm on a polypropylene (PP) filter (Whatman, 7002-0290) or polytetrafluoroethylene (PTFE) filter (ADVANTEC MFS, 102968-892) at room temperature using a casting knife. The casted nascent polymer film was immersed immediately into an aqueous coagulation bath containing HmIm with varying concentrations (0.0 M, 0.5 M, 1.0 M, 1.5 M, and 2.0 M) in 150 ml DI water. The resulting membrane sample was kept into the coagulation bath for 1 hr and moved to a MeOH solution for solvent exchange. After 1 hr in the MeOH solution, the sample was slowly dried under a nearly saturated environment with MeOH for 48 hrs. The resulting membrane was measured at ca. 130 ± 10 μm in thickness and stored in a petri dish for characterization and testing. For a comparison purpose, a conventional MMM with ca. 20 wt% ZIF-8 loading was prepared using a priming and blending method. ZIF-8 particles were prepared by following a procedure described elsewhere [16]. A ZIF-8/solvent suspension was prepared by dispersing the ZIF-8 particles in THF in a sonication bath. Afterward, a small amount of 6FDA-DAM (10 wt% of the total polymer in MMMs) was added into the ZIF-8 suspension and stirred for 6 h. The remaining polymer was added into the suspension and further stirred overnight on a lab shaker. Once the mixture solution became homogeneous, it was casted on a glass plate and covered with aluminum foil. The solvent was slowly evaporated at room temperature for 2 days. Samples are fully dried before the gas separation tests to remove residuals. The membrane was determined ca. 280 μm thick.

2.3. Characterizations

Scanning electron microscope (SEM) images were taken using a JEOL JSM-7500F at acceleration voltage of 5 keV and working distance of 15 mm. Transmission electron microscopy (TEM) analysis was conducted using a FEI Tecnai G2 F20 Super-Twin FE-TEM operating at 120 keV. TEM samples were prepared using a Tescan LYRA-3 Model GMH dual-beam FIB instrument. X-ray diffraction (XRD) patterns were collected using a Miniflex II diffractometer (Rigaku) with Cu-Kα radiation ($\lambda = 1.5406$ Å) in the 2 θ range of 5–40°. A Nicolet iS5 spectrophotometer equipped with iD7 ATR (Thermo Scientific) was used to obtain attenuated total reflectance Fourier transform infrared (ATR-FTIR) spectra at a resolution of 5 cm^{-1} with 16 scans in the span of 4000–400 cm^{-1}. Thermogravimetric analysis (TGA) was performed using Q50 (TA instruments) in the temperature range of 25 °C to 800 °C at the heating rate of 10 °C min^{-1} under air flow of 60 cm^3 min^{-1}. N_2 adsorption isotherms were taken using ASAP 2020 plus (Micromeritics) at 77 K.

2.4. Gas permeation measurements

An equimolar binary propylene/propane separation performance of the membranes were performed using the Wicke-Kallenbach technique at room temperature under atmospheric pressure. A feed gas mixture was provided at the total flow rate of 100 cm^3 min^{-1}. Argon sweeping gas was flowed onto the permeate side at the same flow rate of the feed gas. A membrane was placed in a custom-made permeation cell and sealed with rubber rings. The composition of the permeate was detected using a gas chromatography (GC 7890A, Agilent) equipped with a flame ionized detector (FID) and a HP-plot Q column. For the long-term performance test, membranes were loaded in the permeation cell and placed under the ambient environment. Their gas separation performances were measured after 10, 20, 30, 50, 70, and 100 days.

3. Results and discussion

The proposed novel MMM fabrication strategy, phase-inversion in sync with metal–organic framework formation (PIMOF), is based on the *in-situ* formation of ZIF-8 nanoparticles concurring with the formation of an asymmetric polymer film by phase inversion. It is noted that the phase inversion technique has been widely used to prepare commercial asymmetric polymer membranes (both flat and hollow fibers) [17,18]. Fig. 1 illustrates how an asymmetric MMM is prepared using the PIMOF process. First, a zinc-containing polymer solution is prepared by adding a proper amount of a zinc source to a 6FDA-DAM (4,4-(Hexafluoroisopropylidene) diphthalic anhydride 2,4,6-trimethyl-1,3-

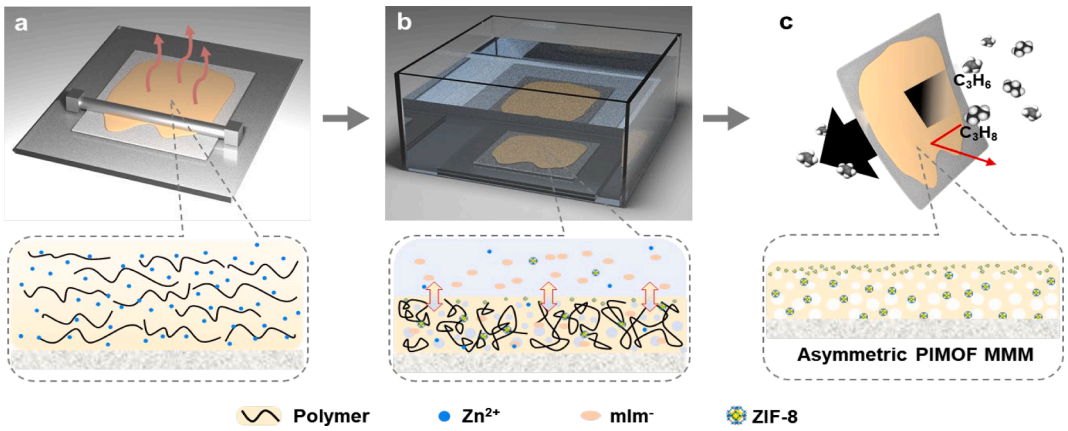

Fig. 1. Schematic illustration of the facile formation of an asymmetric MMM by the PIMOF process: (a) casting a polymer solution containing zinc ions on a porous polymer support, (b) phase inversion by immersion precipitation in a coagulation bath involving HmIm ligands concurring with the *in-situ* formation of ZIF-8 particles inside the polymer, and (c) slow drying.

phenylenediamine) solution (Fig. 1a). The zinc-containing polymer solution is then casted on a porous polymeric support with a casting knife. Volatile components are partially evaporated for a short time, making the top layer more concentrated with polymer than the bottom layer, which eventually facilitates the formation of an asymmetric membrane (i.e., a skin layer on top of a bottom porous layer) (Fig. 1a). As the casted nascent polymer film is immersed into a coagulation bath containing 2-methylimidazole (hereafter, HmIm) ligands, phase inversion is induced by liquid–liquid demixing (Fig. 1b). As shown in the bottom illustration of Fig. 1b, the solvent in the nascent polymer film is replaced by the non-solvent in the coagulation bath. This leads to the solidification of the polymer film by polymer chain entanglement and thereby to the formation of an asymmetric structure [19]. In sync with this polymer phase-inversion, the zinc ions in the polymer film and the HmIm in the coagulation bath diffuse in the opposite direction (i.e., counter-diffusion), thereby enabling the *in-situ* formation of ZIF-8 filler particles inside the polymer film (see the bottom illustration of Fig. 1b). The diffusion of the ligands into the polymer is much faster than that of the zinc ions into the coagulation bath since the ligands diffuse along with the non-solvent invading into the polymer film. This results in the formation of ZIF-8 particles mostly inside the polymer film. The resulting 6FDA-DAM/ZIF-8 MMM exhibits an asymmetric structure with a selective dense mixed-matrix top layer on a porous bottom layer (bottom illustration of Fig. 1c). The PIMOF process is highly scalable since it resembles widely used phase-inversion processes in commercial polymer membrane manufacturing [20].

The composition of the polymer solution is of critical importance in order to obtain a defect-free dense skin layer on top of a porous layer in an asymmetric membrane [19,21]. Since the polymer solution must be in a single phase (black square dots) not two phases (blue square dots),

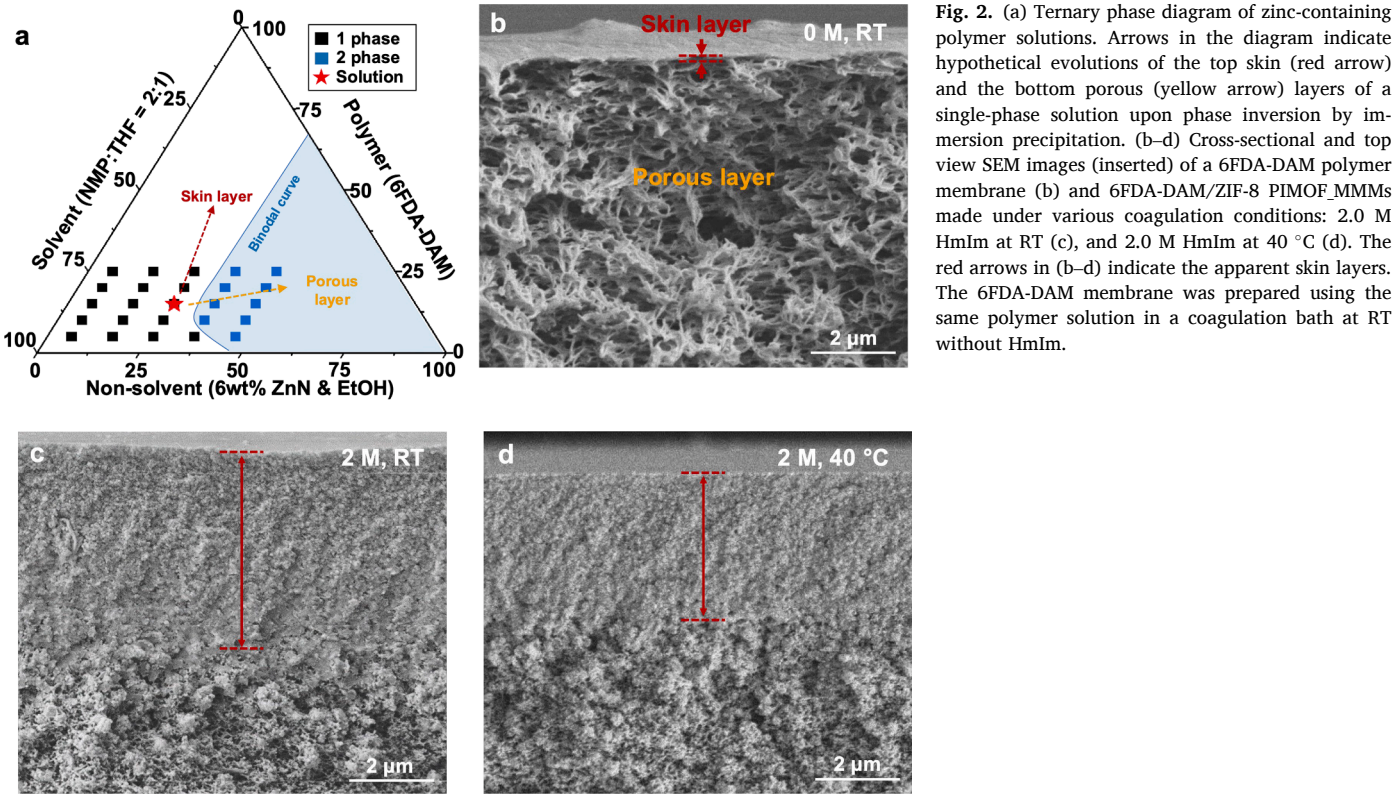

Fig. 2. (a) Ternary phase diagram of zinc-containing polymer solutions. Arrows in the diagram indicate hypothetical evolutions of the top skin (red arrow) and the bottom porous (yellow arrow) layers of a single-phase solution upon phase inversion by immersion precipitation. (b–d) Cross-sectional and top view SEM images (inserted) of a 6FDA-DAM polymer membrane (b) and 6FDA-DAM/ZIF-8 PIMOF_MMMs made under various coagulation conditions: 2.0 M HmIm at RT (c), and 2.0 M HmIm at 40 °C (d). The red arrows in (b–d) indicate the apparent skin layers. The 6FDA-DAM membrane was prepared using the same polymer solution in a coagulation bath at RT without HmIm.

the ternary polymer/solvent/non-solvent system was carefully investigated by varying the composition of the solution, thereby determining the binodal line (the blue dotted line) in a ternary phase diagram. As shown in the phase diagram (Fig. 2a), the polymer concentration was set at 15 wt% that exhibited a proper viscosity [22]. If the concentration is too high, the solution becomes too viscous, consequently difficult to process. An allotted amount of 6FDA-DAM polymer was dissolved in two miscible solvents, non-volatile 1-methyl-2-pyrrolidone (NMP) and volatile tetrahydrofuran (THF), with 2:1 ratio by weight [23,24]. Since zinc nitrate hexahydrate (hereafter, ZnN) serves as a non-solvent additive, the maximum ZnN loading in the polymer/solvent system was 8 wt%. In other words, too much ZnN led to undesirable phase separation. As such, the concentration of ZnN was fixed at 6 wt% (Fig. 2a). Once casted, the volatile solvent and non-solvent (i.e., THF and EtOH, respectively) evaporate from the casted nascent polymer film, leading to the relatively high polymer concentration in the top layer, which then evolves in the single-phase region in the coagulation bath (see the red arrow in Fig. 2a). On the other hand, the composition of the bottom layer is such that it goes through spinodal decomposition phase separation in the coagulation bath, forming continuous pore channels (see the yellow arrow in Fig. 2a). This separate evolution of the top and bottom layers of the nascent polymer film is critical to form a defect-free skin layer on top of a porous layer (Fig. 2a) [19].

Due to the counter diffusion of zinc ions in the nascent polymer film and HmIm in the coagulation bath, ZIF-8 filler particles form *in-situ* inside the polymer film concurring with polymer phase-inversion. Fig. 2b and c show the electron micrographs of a 6FDA-DAM membrane without HmIm in the coagulation bath and a 6FDA-DAM/ZIF-8 MMM formed by the PIMOF process (hereafter, PIMOF_MMMs) with 2.0 M HmIm concentration in the coagulation bath at room temperature (RT). Several observations can be made. First, both polymer membrane and MMM show asymmetric structures (see Fig. 2b-c and S1). While the polymer membrane displays a submicron thick skin layer, a several micron thick skin layer was observed for the PIMOF_MMM possibly owing to the decrease in the phase inversion rate in the presence of HmIm. The strong repulsive interactions between polymer and non-solvent (i.e., water) could be compromised by adding HmIm in the aqueous coagulation bath, thereby decreasing the phase inversion rate. Consequently, the PIMOF_MMM shows a thicker skin layer than the polymer membrane. As the HmIm concentration in the coagulation bath increases, the thickness of the skin layer keeps at *ca.* 4 – 6 μm (Fig. S1). The top-view SEM images (see Fig. S1) show a smooth surface without macroscopic pinhole defects. On the other hand, when the coagulation bath temperature was raised from RT to 40 °C, the diffusion of the non-solvent was promoted, thereby enhancing phase inversion [25] and consequently reducing the thickness of the apparent skin layer (Fig. 2d). When the bath temperature was further raised to 60 °C, however, the porous layer was partially collapsed and undesirable pinholes on the skin layer were formed (Fig. S2) [26,27].

Fig. 3a presents the XRD patterns of the PIMOF_MMMs prepared with varying linker concentrations and temperatures of coagulation baths. The diffraction patterns of the PIMOF_MMMs were consistent with that of ZIF-8, confirming the *in-situ* formation of ZIF-8 filler particles inside the polymer in sync with polymer phase inversion (Fig. 3a). It is worthy of noting that the ZIF-8 fillers were mostly formed inside the polymer films rather than on the membrane surface (see inset images in Fig. 2c-d and S3). Furthermore, there were few ZIF-8 particles found in the coagulation bath (Fig. S3). This is likely due to the fact that the diffusion of HmIm into the polymer is much faster than that of zinc ions into the coagulation solution due to 1) the diffusion of the charged zinc ions requires charge-balancing anions [28] and 2) the diffusion of HmIm can be assisted by the infusion of the non-solvent into the polymer [29].

The total ZIF-8 filler loadings in the PIMOF MMMs were determined using thermal gravimetric analysis (TGA) (Figs. S4 and S6). As the HmIm concentration in the coagulation bath increased from 0.0 M to 0.5 M, 1.0 M, 1.5 M, and 2.0 M, the total ZIF-8 loadings in the PIMOF_MMMs increased linearly (Fig. S6), which is consistent with the XRD observation (Fig. 3a). The highest total ZIF-8 loading was estimated ca. 15 wt% at 2.0 M of the linker concentration and 40 °C of the bath temperature. It is noted that the total ZIF-8 loading includes filler particles formed in the skin layer as well as those in the bottom porous layer. As shown in Figs. S5 and S6, the EDS mapping of the PIMOF_MMMs clearly revealed relatively strong Zn signals at the top layer of *ca.* 5 μm, strongly suggesting higher ZIF-8 loadings in the top layer than in the porous bottom layer. Using the TGA analysis combined with the EDS elemental analysis, the average ZIF-8 loadings in the top *ca.* 5 μm layers were estimated by the overall ZIF-8 loadings from TGA analysis multiplied by the ratio of the average zinc counts in the top *ca.* 5 μm layers to that through the entire membrane cross-section from the EDS line scan (Figs. S5-6, Table S1). The result is as high as ca. 55.6 wt%, much higher than the

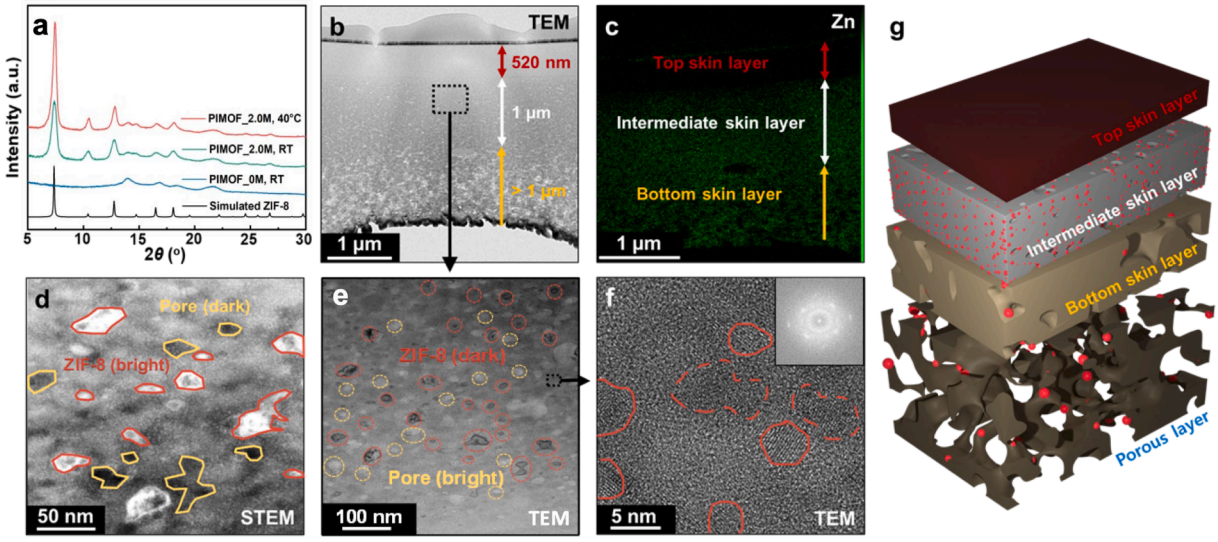

Fig. 3. (a) XRD patterns of MMMs with different ligand concentrations in the coagulation bath in comparison with that of a mmm prepared by a conventional blending method. Those in the parentheses present the ligand concentrations in the coagulation bath and the bath temperature and 0.0 M represents a pure 6FDA-DAM membrane. (b) TEM image of the cross-section of the PIMOF_MMM (2.0 M, 40 °C). (c) Zn EDS elemental mapping image of the same sample as shown in (b). (d) STEM image and (e) TEM image of the intermediate skin layer. (f) HRTEM image of the ZIF-8 particles in the intermediate skin layer and the corresponding FFT pattern (inset). (g) Illustration of the overall microstructure of the PIMOF_MMM.

total ZIF-8 loading. It is noteworthy to mention that despite the relatively large consumption of HmIm per membrane area in this study, the possibility to optimize dimensions of a water bath and the high-capacity processing high filer loading MMMs continuously with the high reproducibility can make the process economically preferable.

To investigate the microstructure of the ZIF-8-containing skin layers, TEM and STEM analyses were performed on the PIMOF_MMM prepared in a coagulation bath containing 2.0 M of HmIm at 40 °C (hereafter, PIMOF_MMM (2.0 M, 40 °C)). Fig. 3b presents the TEM image of the top *ca.* 3 μm thick skin layer of the membrane. The TEM sample was prepared by focused ion beam (FIB) lift-out technique. The image reveals the presence of three distinct layers within the skin layer: 1) a top skin layer of *ca.* 520 nm in thickness, 2) a *ca.* 1 μm thick intermediate skin layer, and 3) a bottom skin layer. The top skin layer appears to be dense with little zinc signals in the TEM-EDS mapping (see Fig. 3c), indicating no ZIF-8 fillers formed in this layer. This is likely due to the fact that the zinc ions trapped in the top skin layer were mostly washed out before forming ZIF-8 filler particles due to the shorter diffusion length during phase inversion (i.e., the diffusion time scale is shorter than the reaction time scale). Fig. 3d and 3e present a STEM image and a TEM image of regions in the intermediate skin layer between the top skin layer and the bottom skin layer. As can be seen in the figures, there are many nano-sized (*ca.* 5 nm) bright and dark spots with a uniform spherical shape in the STEM and the TEM images, respectively, besides the relatively large (ca. 10–50 nm) and irregular areas. Fig. 3f presents a TEM image of one such darker spot that shows particles consisting of a few coalesced nanocrystals of < *ca.* 5 nm in size (see red dotted closed contours in the figure). The corresponding fast Fourier transform (FFT) confirms the dark spots enclosed in red lines in Fig. 3e are ZIF-8 nanocrystals and their coalesced particles. It is noted that the typical MOF/ZIF filler particle sizes for MMMs are in the range of *ca.* 20–100 nm [10]. As such, the filler size of <*ca.* 5 nm is unprecedented for MMMs. Fig. 3e also shows dark (STEM) and bright (TEM) regions of ca. 10 ~ 20 nm that are irregular in size and shape, which correspond to mesopores. The pores are much smaller in size than the thickness of the intermediate skin layer and are relatively sparsely dispersed in the layer. Judging from these observations, the pores in the intermediate skin layer seem non-continuous, formed along the nucleation and growth path during the phase inversion. In other words, the pores in the intermediate skin layer are not likely short-circuiting gas transport, rather enhancing gas transport by effectively reducing the skin layer thickness. Though further studies are necessary, formation of the smaller and the bigger ZIF-8 particles in the intermediate skin layer are likely due to the two different formation mechanisms: the sub-5 nm particles are formed in the confined spaces instantly upon the solidification of polymer, whereas the bigger particles are prepared in the spaces initially formed as non-continuous pores. On the other hand, the bottom skin layer shows a lot more pores (cavities) that are much bigger and more importantly interconnected (Fig. S7).

Fig. 4 presents the N_2 adsorption isotherm of the PIMOF_MMM (2.0 M, RT) in comparison with those of ZIF-8 powder and a ZIF-8-containing MMM prepared by a conventional blending method (hereafter, blended MMM). A couple of observations can be made. First, as shown in Fig. 4a, the pore volume of the PIMOF_MMM is much smaller than that of the ZIF-8 powder due to the non-porous polymer phase in the PIMOF_MMM (note that the specific uptake is presented in a log–log scale). Meanwhile, the PIMOF_MMM exhibits significantly larger pore volume than the blended MMM despite its lower total ZIF-8 loading (13 wt% vs 20 wt %). This can be attributed to the much shorter diffusion length of the PIMOF_MMM since it is asymmetric with a much thinner skin layer consisting of a top dense layer, an intermediate semi-porous layer and a bottom porous layer (*ca.* 5 μm) than the blended MMM (*ca.* 280 μm) (see Fig. S8). Second, as can be seen in Fig. 4b, the ZIF-8 powder and the blended MMM clearly show typical two-step gate-opening phenomena at the relative pressures of *ca.* 0.004/ *ca.* 0.02 and *ca.* 0.007/ *ca.* 0.02, respectively (see dotted rectangles in Fig. 4b) [30]. In a stark contrast, the PIMOF_MMM exhibits no apparent gate opening possibly due to the restricted swing motion of the mIm linkers resulting from relatively strong interaction with polymer chains. Another interesting observation is that at low relative pressures ($p/p0(10^{-4})$, the PIMOF_MMM exhibits much higher gas uptake, strongly suggesting that it possesses more high-energy adsorption sites. The presence of these high-energy adsorption sites might be due to the unprecedentedly small sub-5 nm ZIF-8 filler nanoparticles with much greater surface-to-volume ratio. These high-energy surfaces of the ZIF-8 nanofillers are expected to result in the much stronger interaction between the fillers and the polymer than typical ZIF-8 filler particles, thereby considerably affecting the swing motion of the linkers and consequently the molecular sieving properties of the ZIF-8 nanofillers [31].

Fig. 5a and Tables S2-S3 present the binary propylene/propane (C3) separation performances of the PIMOF_MMMs in comparison with other membranes including MMMs prepared by a conventional blending method and the PMMOF [32]. It is noted that the permeance/selectivity upper bound in Fig. 5a is based on the permeability/selectivity upper bound [33] with an assumption of the thickness of 1 μm. The C3 separation performances of the PIMOF_MMMs were considerably affected by the processing conditions such as linker concentration and phase inversion temperature. As the HmIm concentration in the coagulation bath increased, both the C_3H_6 permeance and the separation factor of the PIMOF_MMMs increased due to the increased ZIF-8 loading (Fig. 5a and Table S2). The increase in the C_3H_6 permeance was somewhat modest as compared to that in the separation factor, which was attributed to the changing thicknesses of the skin layers at different phase inversion conditions (see SEM images in Fig. 2c and S1). At the HmIm

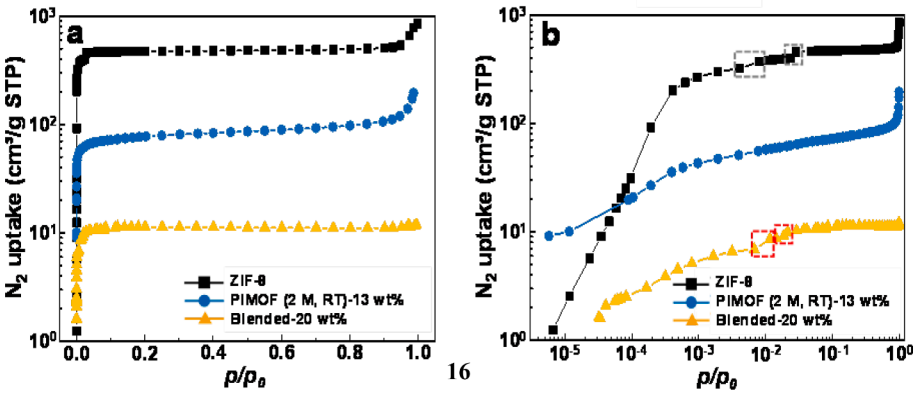

Fig. 4. N_2 adsorption isotherm at 77 K of a PIMOF_MMM (2M, RT) in comparison with those of ZIF-8 and (a) conventionally prepared MMM with 20 wt% ZIF-8 loading: (a) linear-log scale and (b) log–log scale.

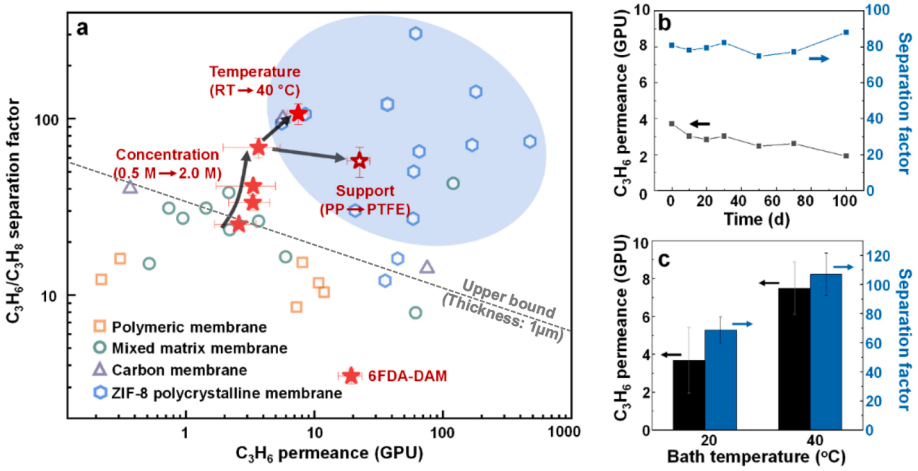

Fig. 5. (a) The C3 separation performances of the PIMOF_MMMs in comparison with other membranes. All PIMOF_MMMs presented here are made on pp supports except one on PTFE (ADVANTEC MFS, 102968–892) supports. (b) Time-dependent C3 separation performance of the PIMOF MMMs (2 M, RT). (c) C3 separation performance of the PIMOF MMMs (2 M) at the different coagulation bath temperatures. All the membranes are tested at RT under atmospheric pressure (equimolar binary C_3H_6/C_3H_8).

concentration of 2.0 M, the PIMOF_MMMs (2 M, RT) show surprisingly high C3 separation performances with the C_3H_6 permeance of 3.68 ± 1.73 GPU and the average C3 separation factor of 68.72 ± 8.93. It is noted that the conventionally-prepared ZIF-8-containing MMMs showed C_3H_6/C_3H_8 separation factors as high as *ca.* 31.1 [34] while the MMMs by the PMMOF exhibited C3 separation factors of ca. 38.04 [15]. The C_3H_6 permeabilities are not reported because it was difficult to precisely determine the thickness of the active separation layer (i.e., intermediate skin layer) due to the ambiguous boundary between the intermediate skin layer and the bottom skin layer [26].

When the coagulation bath temperature was raised to 40 °C, the resulting PIMOF_MMMs showed the dramatically enhanced C3 separation performance (Fig. 5c). The PIMOF_MMMs (2.0 M, 40 °C) show unprecedentedly high C3 separation performances with the C_3H_6 permeance of 7.48 ± 1.39 GPU and the average C3 separation factor of 106.93 ± 14.42, respectively. The faster phase inversion rate at the higher temperature resulted in forming a thinner apparent skin layer (Fig. 2c-d), consequently increasing the C_3H_6 permeance. Furthermore, the higher temperature accelerated the *in-situ* formation of ZIF-8 filler nanoparticles, thereby increasing the ZIF-8 loading in the skin layer (>50 % at 40 °C vs > 40 wt% at RT). It is reminded that when the coagulation bath temperature was further raised to 60 °C, the resulting membranes showed pinholes as well as many particles formed on the membrane surface (Fig. S2), resulting in poor separation performances.

As shown in Fig. 5a, the C3 separation performances of the PIMOF_MMMs are comparable even with some of the best-performing polycrystalline ZIF-8 membranes [35–45]. The unexpectedly high C3 separation performances of the PIMOF_MMMs are ascribed likely to 1) the uniform distribution of the unprecedentedly small ZIF-8 nanoparticles (<5 nm), 2) the high ZIF-8 loadings in the intermediate layers (>50 wt%), and 3) the enhanced molecular sieving property of the ZIF-8 nanofillers resulting from the restricted linker swing motion. In addition, despite the increase in separation factor and decrease in permeance likly owing to an aging effect of polymer [46], the PIMOF_MMMs show relatively stable separation performances over several months (Fig. 5b).

Finally, changing the polymeric support from polypropylene (PP) to polytetrafluoroethylene (PTFE) increased the C_3H_6 permeance significantly from 3.68 ± 1.73 GPU to 22.45 ± 4.49 GPU while maintaining relatively high C3 separation factor (57.68 ± 11.17) (Fig. 5a). Detail studies of the support effect on the performances of PIMOF_MMMs are currently underway and will be reported in near future.

4. Conclusions

In conclusion, we have successfully demonstrated a new facile *in-situ* MMM fabrication process, coined as phase-inversion in sync with MOF formation (PIMOF). The PIMOF could effectively address most of the issues of current MMMs for their commercial applications. Concurring with polymer phase-inversion, ZIF-8 filler particles formed *in-situ* inside the top polymer layers by the counter-diffusion of zinc ions and ligands and subsequent crystallization. Microstructural analysis revealed the presence of the separation-relevant micron-thick intermediate skin layers that contained unprecedentedly small ZIF-8 nanoparticles that were uniformly distributed in the layers. Further investigations into the properties of the distinct skin layers will be carried out in future studies. Ligand concentrations and coagulation bath temperatures were found to have significant effects on the phase-inversion and ZIF-8 formation, thereby affecting the separation performances of the PIMOF MMMs. The PIMOF_MMMs showed the unprecedentedly high C_3H_6/C_3H_8 separation performances with the C_3H_6 permeance and the C_3H_6/C_3H_8 separation factor of as high as ca. 7.5 GPU and ca. 107, respectively. The PIMOF MMMs significantly outperform all reported polymer membranes, MMMs, and carbon molecular sieve membranes and are comparable even with high-performance polycrystalline ZIF-8 membranes. The unexpectedly high separation performances of the PIMOF MMMs were attributed likely due to the enhanced molecular sieving properties of ZIF-8 nanofillers that are unprecedentedly small in size (<5 nm) along with the high ZIF-8 loading (>50 wt%) in the skin layer. We expect the PIMOF process to be a significant breakthrough toward bringing MMMs for commercial gas separations including C_3H_6/C_3H_8 separation.

Declaration of Competing Interest

The authors declare that they have no known competing financial interests or personal relationships that could have appeared to influence the work reported in this paper.

Data availability

No data was used for the research described in the article.

Acknowledgements

H.-K.J. acknowledges the financial support from the National Science Foundation (CBET-1929596). This publication was made possible in part by NPRP grant # 12S-0209-190064 from the Qatar National Research Fund (a member of Qatar Foundation). The findings achieved herein are solely the responsibility of the authors. The National Science Foundation supported the FE-SEM acquisition under Grant DBI-0116835, the VP for Research Office, and the Texas A&M Engineering Experimental Station. K. Y. Cho acknowledges financial support through the National Research Foundation of Korea (NRF) grant funded by the

Korea government (MSIT) (No.NRF-2022R1C1C1003313).

Appendix A. Supplementary data

Supplementary data to this article can be found online at https://doi.org/10.1016/j.cej.2023.143048.

References

[1] W.J. Koros, Gas separation membranes: needs for combined materials science and processing approaches, Macromol. Symp. 188 (1) (2002) 13–22, https://doi.org/10.1002/1521-3900(200211)188:1<13::AID-MASY13>3.0.CO;2-W.

[2] D.S. Sholl, R.P. Lively, Seven chemical separations to change the world, Nature 532 (7600) (2016) 435–437, https://doi.org/10.1038/532435a.

[3] R.W. Baker, Future directions of membrane gas separation technology, Ind Eng Chem Res 41 (6) (2002) 1393–1411, https://doi.org/10.1021/ie0108088.

[4] L.M. Robeson, The upper bound revisited, J. Membr. Sci. 320 (1) (2008) 390–400, https://doi.org/10.1016/j.memsci.2008.04.030.

[5] R. Sidhikku Kandath Valappil, N. Ghasem, M. Al-Marzouqi, Current and future trends in polymer membrane-based gas separation technology: A comprehensive review, Journal of Industrial and Engineering Chemistry 98 (2021) 103-129. 10.1016/j.jiec.2021.03.030.

[6] W.J. Koros, C. Zhang, Materials for next-generation molecularly selective synthetic membranes, Nat. Mater. 16 (3) (2017) 289–297, https://doi.org/10.1038/nmat4805.

[7] M.R.A. Hamid, H.K. Jeong, Recent advances on mixed-matrix membranes for gas separation: Opportunities and engineering challenges, Korean J Chem Eng 35 (8) (2018) 1577–1600, https://doi.org/10.1007/s11814-018-0081-1.

[8] H. Yehia, T. Pisklak, J. Ferraris, K. Balkus, I. Musselman, Methane facilitated transport using copper (II) biphenyl dicarboxylate-triethylenediamine/poly (3-acetoxyethylthiophene) mixed matrix membranes, Abstracts of Papers of the American Chemical Society, AMER CHEMICAL SOC 1155 16TH ST, NW, WASHINGTON, DC 20036 USA, 2004, pp. U351-U351.

[9] M. Galizia, W.S. Chi, Z.P. Smith, T.C. Merkel, R.W. Baker, B.D. Freeman, 50th Anniversary Perspective: Polymers and Mixed Matrix Membranes for Gas and Vapor Separation: A Review and Prospective Opportunities, Macromolecules 50 (20) (2017) 7809–7843, https://doi.org/10.1021/acs.macromol.7b01718.

[10] G. Dong, H. Li, V. Chen, Challenges and opportunities for mixed-matrix membranes for gas separation, J. Mater. Chem. A 1 (15) (2013) 4610–4630, https://doi.org/10.1039/C3TA00927K.

[11] J.-J. Qin, J. Gu, T.-S. Chung, Effect of wet and dry-jet wet spinning on the shear-induced orientation during the formation of ultrafiltration hollow fiber membranes, J. Membr. Sci. 182 (1) (2001) 57–75, https://doi.org/10.1016/S0376-7388(00)00552-4.

[12] L.Y. Jiang, T.S. Chung, C. Cao, Z. Huang, S. Kulprathipanja, Fundamental understanding of nano-sized zeolite distribution in the formation of the mixed matrix single- and dual-layer asymmetric hollow fiber membranes, J. Membr. Sci. 252 (1–2) (2005) 89–100, https://doi.org/10.1016/j.memsci.2004.12.004.

[13] A.M. Marti, S.R. Venna, E.A. Roth, J.T. Culp, D.P. Hopkinson, Simple Fabrication Method for Mixed Matrix Membranes with in Situ MOF Growth for Gas Separation, ACS Appl. Mater. Interfaces 10 (29) (2018) 24784–24790, https://doi.org/10.1021/acsami.8b06592.

[14] S. He, B. Zhu, X. Jiang, G. Han, S. Li, C.H. Lau, Y. Wu, Y. Zhang, L. Shao, Symbiosis-inspired de novo synthesis of ultrahigh MOF growth mixed matrix membranes for sustainable carbon capture, Proceedings of the National Academy of Sciences 119 (1) (2022) e2114964119. 10.1073/pnas.2114964119.

[15] S. Park, M.R.A. Hamid, H.K. Jeong, Highly Propylene-Selective Mixed-Matrix Membranes by in Situ Metal Organic Framework Formation Using a Polymer-Modification Strategy, Acs Appl Mater Inter 11 (29) (2019) 25949–25957.

[16] S. Park, H.-K. Jeong, In-situ linker doping as an effective means to tune zeolitic-imidazolate framework-8 (ZIF-8) fillers in mixed-matrix membranes for propylene/propane separation, J. Membr. Sci. 596 (2020), 117689, https://doi.org/10.1016/j.memsci.2019.117689.

[17] P. Sukitpaneenit, T.-S. Chung, Chapter 16 - Molecular elucidation of morphology and mechanical properties of PVDF hollow fiber membranes from aspects of phase inversion, crystallization, and rheology☆, in: T.-.-S. Chung, Y. Feng (Eds.), Hollow Fiber Membranes, Elsevier, 2021, pp. 333–360, https://doi.org/10.1016/B978-0-12-821876-1.00013-5.

[18] I. Pinnau, W.J. Koros, Structures and gas separation properties of asymmetric polysulfone membranes made by dry, wet, and dry/wet phase inversion, J. Appl. Polym. Sci. 43 (8) (1991) 1491–1502, https://doi.org/10.1002/app.1991.070430811.

[19] J.G. Wijmans, J. Kant, M.H.V. Mulder, C.A. Smolders, Phase separation phenomena in solutions of polysulfone in mixtures of a solvent and a nonsolvent: relationship with membrane formation, Polymer 26 (10) (1985) 1539–1545, https://doi.org/10.1016/0032-3861(85)90090-4.

[20] C.Y. Feng, K.C. Khulbe, T. Matsuura, A.F. Ismail, Recent progresses in polymeric hollow fiber membrane preparation, characterization and applications, Sep. Purif. Technol. 111 (2013) 43–71, https://doi.org/10.1016/j.seppur.2013.03.017.

[21] J.-J. Shieh, T.S. Chung, Effect of liquid-liquid demixing on the membrane morphology, gas permeation, thermal and mechanical properties of cellulose acetate hollow fibers, J. Membr. Sci. 140 (1) (1998) 67–79, https://doi.org/10.1016/s0376-7388(97)00267-6.

[22] S.S. Hosseini, N. Peng, T.S. Chung, Gas separation membranes developed through integration of polymer blending and dual-layer hollow fiber spinning process for hydrogen and natural gas enrichments, J. Membr. Sci. 349 (1–2) (2010) 156–166, https://doi.org/10.1016/j.memsci.2009.11.043.

[23] C.-C. Chen, W. Qiu, S.J. Miller, W.J. Koros, Plasticization-resistant hollow fiber membranes for CO2/CH4 separation based on a thermally crosslinkable polyimide, J. Membr. Sci. 382 (1–2) (2011) 212–221, https://doi.org/10.1016/j.memsci.2011.08.015.

[24] G. Dong, H. Li, V. Chen, Factors affect defect-free Matrimid® hollow fiber gas separation performance in natural gas purification, J. Membr. Sci. 353 (1–2) (2010) 17–27, https://doi.org/10.1016/j.memsci.2010.02.012.

[25] L. Jiang, Fabrication of Matrimid/polyethersulfone dual-layer hollow fiber membranes for gas separation, J. Membr. Sci. 240 (1–2) (2004) 91–103, https://doi.org/10.1016/j.memsci.2004.04.015.

[26] C. Zhang, K. Zhang, L. Xu, Y. Labreche, B. Kraftschik, W.J. Koros, Highly scalable ZIF-based mixed-matrix hollow fiber membranes for advanced hydrocarbon separations, AIChE J 60 (7) (2014) 2625–2635, https://doi.org/10.1002/aic.14496.

[27] H. Zhang, X. Lu, Z. Liu, Z. Ma, S. Wu, Z. Li, X. Kong, J. Liu, C. Wu, The unidirectional regulatory role of coagulation bath temperature on cross-section radius of the PVDF hollow-fiber membrane, J. Membr. Sci. 550 (2018) 9–17, https://doi.org/10.1016/j.memsci.2017.12.059.

[28] S.P. Lee, J.F. Nicholls, Diffusion of charged ions in mucus gel: effect of net charge, Biorheology 24 (6) (1987) 565–569, https://doi.org/10.3233/bir-1987-24607.

[29] H.L.C. Maganto, M.B.M.Y. Ang, G.V.C. Dizon, A.R. Caparanga, R.R. Aquino, S.-H. Huang, H.-A. Tsai, K.-R. Lee, Infusion of Silver-Polydopamine Particles into Polyethersulfone Matrix to Improve the Membrane's Dye Desalination Performance and Antibacterial Property, Membranes 11 (3) (2021) 216.

[30] D. Fairen-Jimenez, S.A. Moggach, M.T. Wharmby, P.A. Wright, S. Parsons, T. Duren, Opening the Gate: Framework Flexibility in ZIF-8 Explored by Experiments and Simulations, J Am Chem Soc 133 (23) (2011) 8900–8902, https://doi.org/10.1021/ja202154j.

[31] S. Friebe, B. Geppert, F. Steinbach, J. Caro, Metal-Organic Framework UiO-66 Layer: A Highly Oriented Membrane with Good Selectivity and Hydrogen Permeance, Acs Appl Mater Inter 9 (14) (2017) 12878–12885, https://doi.org/10.1021/acsami.7b02105.

[32] S. Park, M.R. Abdul Hamid, H.-K. Jeong, Highly Propylene-Selective Mixed-Matrix Membranes by in Situ Metal–Organic Framework Formation Using a Polymer-Modification Strategy, ACS Applied Materials & Interfaces 11(29) (2019) 25949-25957. 10.1021/acsami.9b07106.

[33] R.L. Burns, W.J. Koros, Defining the challenges for C3H6/C3H8 separation using polymeric membranes, J. Membr. Sci. 211 (2) (2003) 299–309, https://doi.org/10.1016/S0376-7388(02)00430-1.

[34] X. Ma, R.J. Swaidan, Y. Wang, C.-E. Hsiung, Y. Han, I. Pinnau, Highly Compatible Hydroxyl-Functionalized Microporous Polyimide-ZIF-8 Mixed Matrix Membranes for Energy Efficient Propylene/Propane Separation, ACS Applied Nano Materials 1 (7) (2018) 3541–3547, https://doi.org/10.1021/acsanm.8b00682.

[35] K. Huang, Z. Dong, Q. Li, W. Jin, Growth of a ZIF-8 membrane on the inner-surface of a ceramic hollow fiber via cycling precursors, Chem. Commun. 49 (87) (2013) 10326, https://doi.org/10.1039/c3cc46244g.

[36] Y. Pan, W. Liu, Y. Zhao, C. Wang, Z. Lai, Improved ZIF-8 membrane: Effect of activation procedure and determination of diffusivities of light hydrocarbons, J. Membr. Sci. 493 (2015) 88–96, https://doi.org/10.1016/j.memsci.2015.06.019.

[37] X. Ma, P. Kumar, N. Mittal, A. Khlyustova, P. Daoutidis, K.A. Mkhoyan, M. Tsapatsis, Zeolitic imidazolate framework membranes made by ligand-induced permselectivation, Science 361 (6406) (2018) 1008–1011, https://doi.org/10.1126/science.aat4123.

[38] R. Wei, H.Y. Chi, X. Li, D. Lu, Y. Wan, C.W. Yang, Z. Lai, Aqueously Cathodic Deposition of ZIF-8 Membranes for Superior Propylene/Propane Separation, Adv. Funct. Mater. 30 (7) (2020) 1907089, https://doi.org/10.1002/adfm.201907089.

[39] E. Barankova, X. Tan, L.F. Villalobos, E. Litwiller, K.-V. Peinemann, A Metal Chelating Porous Polymeric Support: The Missing Link for a Defect-Free Metal-Organic Framework Composite Membrane, Angew. Chem. Int. Ed. 56 (11) (2017) 2965–2968, https://doi.org/10.1002/anie.201611927.

[40] E. Shamsaei, X. Lin, Z.-X. Low, Z. Abbasi, Y. Hu, J.Z. Liu, H. Wang, Aqueous Phase Synthesis of ZIF-8 Membrane with Controllable Location on an Asymmetrically Porous Polymer Substrate, ACS Appl. Mater. Interfaces 8 (9) (2016) 6236–6244, https://doi.org/10.1021/acsami.5b12684.

[41] M.J. Lee, M.R. Abdul Hamid, J. Lee, J.S. Kim, Y.M. Lee, H.-K. Jeong, Ultrathin zeolitic-imidazolate framework ZIF-8 membranes on polymeric hollow fibers for propylene/propane separation, Journal of Membrane Science 559 (2018) 28–34, https://doi.org/10.1016/j.memsci.2018.04.041.

[42] A.J. Brown, N.A. Brunelli, K. Eum, F. Rashidi, J.R. Johnson, W.J. Koros, C. W. Jones, S. Nair, Interfacial microfluidic processing of metal-organic framework hollow fiber membranes, Science 345 (6192) (2014) 72–75, https://doi.org/10.1126/science.1251181.

[43] K. Eum, A. Rownaghi, D. Choi, R.R. Bhave, C.W. Jones, S. Nair, Fluidic Processing of High-Performance ZIF-8 Membranes on Polymeric Hollow Fibers: Mechanistic Insights and Microstructure Control, Adv. Funct. Mater. 26 (28) (2016) 5011–5018, https://doi.org/10.1002/adfm.201601550.

[44] O. Kwon, M. Kim, E. Choi, H. Bae Jun, S. Yoo, C. Won Jong, H. Kim Yun, H. Shin Ju, S. Lee Jong, W. Kim Dae, High–aspect ratio zeolitic imidazolate framework

(ZIF) nanoplates for hydrocarbon separation membranes, Science Advances 8(1) eabl6841. 10.1126/sciadv.abl6841.

[45] S. Zhou, Y. Wei, L. Li, Y. Duan, Q. Hou, L. Zhang, L.-X. Ding, J. Xue, H. Wang, J. Caro, Paralyzed membrane: Current-driven synthesis of a metal-organic framework with sharpened propene/propane separation, Science Advances 4(10) eaau1393. 10.1126/sciadv.aau1393.

[46] S. Song, H. Jiang, H. Wu, M. Zhao, Z. Guo, B. Li, Y. Ren, Y. Wang, C. Ye, M. D. Guiver, G. He, Z. Jiang, Weakly pressure-dependent molecular sieving of propylene/propane mixtures through mixed matrix membrane with ZIF-8 direct-through channels, J. Membr. Sci. 648 (2022), 120366, https://doi.org/10.1016/j.memsci.2022.120366.